Automatika

Journal for Control, Measurement, Electronics, Computing and Communications

ISSN: (Print) (Online) Journal homepage: www.tandfonline.com/journals/taut20

Wearable frequency selective surface-based compact dual-band antenna for 5G and Wi-Fi applications

C. Renit & T. Ajith Bosco Raj

To cite this article: C. Renit & T. Ajith Bosco Raj (2024) Wearable frequency selective surface-based compact dual-band antenna for 5G and Wi-Fi applications, Automatika, 65:2, 454-462, DOI: 10.1080/00051144.2023.2296796

To link to this article: https://doi.org/10.1080/00051144.2023.2296796

Published online: 10 Jan 2024.

AUTOMATIKA
2024, VOL. 65, NO. 2, 454–462
https://doi.org/10.1080/00051144.2023.2296796

Wearable frequency selective surface-based compact dual-band antenna for 5G and Wi-Fi applications

C. Renit[a] and T. Ajith Bosco Raj[b]

[a]Department of ECE, St. Xavier's Catholic College of Engineering, Nagercoil, India; [b]Electronics and Communication Engineering, PSN College of Engineering and Technology, Tirunelveli, India

ABSTRACT

The ever-growing miniaturization of electronic devices is foremost due to a wide range of changes in shrinking the wearable devices. This article focuses on a small, wearable antenna with dual bands for 5G and Wi-Fi communications. The Frequency Selective Surface (FSS) is made of denim Jean and has a top- loaded stubs-inspired radiator and a modified ground plane structure to induce the resonance frequencies at 3.5 and 5.8 GHz within a compact 31.5 mm × 26 mm size. With the FSS integrated antenna, you can cover the N-78 5G band-width of 620 MHz (S11 × −10dB) in the 3.28–3.9 GHz range, as well as the Wi-Fi bandwidth of 600 MHz (S11 × −10 dB) in the range of 5.65–6.25 GHz. The antenna presented has a peak gain of 7.07 dB at 3.5 GHz and 6.02 dB at 5.8 GHz. This antenna is mounted near a human arm model lowering the Specific Absorption Rate (SAR) to 0.370W/kg at 3.5 GHz and 0.870W/kg at 5.8 GHz. The simulated values are validated with measured results and are suitable for body area communication. The designed FSS antenna provides stable impedance bandwidth for conformal applications with enhancing radiation performance.

ARTICLE HISTORY
Received 10 October 2023
Accepted 10 December 2023

KEYWORDS
5G; frequency selective surface (FSS); specific absorption rate (SAR); wearable devices; dual band antenna

1. Introduction

The recent advancement of current wireless communication technologies highlights the requirement for wearable antennas in a wide range of areas such as military applications [1], medical applications, entertainment [2], Internet of Things, personal assistance, security [3] and biomedical telemetric device [4] applications. Keeping the demand for multi-functional devices in mind there are many wearable antennas reviewed in the literature. Nester characters are utilized to provide dual-band operation for Wi-Fi applications [5]. The dual-band operation of 5G and Wi-Fi application is achieved with the help of vertical metal vias in circular patch antenna [6] and double-layer microstrip [7] structure, which has a larger profile. Self-Grounding slit antenna [8] with dual-band operation comes with a larger profile.

A dual-band antenna for off-body communication is achieved by an inverted U-shaped slot at the patch antenna [9] but has a lower gain value. A folded ring antenna [10] and shorting pin at microstrip patch antenna [11] are presented for dual-band operation at body area communication bit it provides a complex structure. Alhough many antennas are presented for wearable applications with acceptable SAR levels, they have lower gain and larger sizes. Metamaterials and frequency selective surfaces are used to reduce SAR levels while increasing antenna gain. A hybrid complementary pair of FSS [12], ring slot FSS [13], square slot FSS [14], and double square slotted FSS [15] is presented for filter applications. Although the resonance is achieved in the desired frequency, the attainment of transmission response bandwidth is low as we take the −20 dB bandwidth.

FSS-integrated antennas aid in minimizing SAR levels while increasing antenna gain. Square loop slot backed U-slot patch antenna along with AMC structure [16] delivers dual-band operation with high gain for ISM band and 5G applications. The triple-layer structure is not a suitable candidate for wearable applications. A square loop-inspired FSS is presented with dual-band operation, which is backed by patch with rectangular spiral and two stubs [17], loading a square loop with a meander stub [18], upper band and lower band element antennas [19], and C-shaped CPW antenna [20]. It improves antenna gain, but the profile of the construction is high and the transmission bandwidth is small. In addition, the bending analysis of antenna with FSS structure is not evident. Furthermore, a wideband antenna FSS [21] is presented to enhance the bandwidth. A micro-strip antenna along with square loop inspired FSS [22–24] is presented for

CONTACT C. Renit renitc.ece@outlook.com Department of ECE, St. Xavier's Catholic College of Engineering, Chunkankadai, Nagercoil 629 003, Tamil Nadu, India

high gain application but the polarization insensitive at different angles of incidence is not carried. So, it is the demand of the research society that compact polarization-insensitive FSS-based wearable antenna with high gain, enhanced bandwidth, low profile, and stable performance under bending conditions is essential.

In this article, top-loaded dual-band wearable antenna with the dimension of 31.5 mm × 26 mm is developed for the applications of 5G and Wi-Fi bands. A unique small wideband square loop-inspired FSS antenna with a unit cell dimension of 38.5 mm × 38.5 mm is developed to reduce SAR and increase gain. This article is structured as follows: Section 2 describes the antenna design and the stages of advancement. Section 3 presents the Frequency-selective surface design with its transmission characteristics. The measured and simulated FSS integrated antenna results are shown in Section 4. Section 5 concludes the article.

2. Antenna design

The top-loaded antenna and frequency selective surface is laser engraved onto a denim Jean substrate. The relative permittivity of the denim Jean substrate is 1.7, and the loss tangent is 0.025. The radiator portion monopole antenna is updated with top loaded structure to produce compact resonance at 3.5 GHz, whereas modification in the ground plane aids in achieving a second resonance at 5.8 GHz. The frequency selective surface inspired by the square loop, [25,26] which works as a band stop filter, is put behind the antenna to limit back radiation and boost gain. Figure 1 depicts the structure of the antenna. Table 1 shows the dimensions of the antenna.

Figure 2(a) shows the design stages of the antenna. The rectangular-shaped monopole antenna is modelled over a jean substrate, which produces resonance at 5.3 GHz. The portion of the radiator is removed and a U-shaped stub is added, as shown in Figure 2(b), which produces resonance at 4.5 GHz. The resonance frequency is further reduced to 3.3 GHz along with 4.5 GHz with the short loop stub, which is added on the top of the monopole structure, as shown in Figure 2(c). A short stub is also inserted on both sides of the ground plane, as shown in Figure 2(d) which covers the dual resonance at 3.5 and 5.8 GHz. To improve impedance matching at 3.5 and 5.8 GHz, a small rectangular section of the ground plane is deleted from the ground portion, as shown in Figure 2(e).

Figure 3 depicts the simulated reflection coefficient for all phases of the proposed antenna. The addition of a U-shaped stub and the addition of a short stub loop structure reduced the resonance frequency from 5.3 to 3.5 GHz. Further addition of a short stub at the ground plane induced dual resonance at the 5G band of 3.5 GHz and Wi-Fi band of 5.8 GHz [27,28]. Furthermore, the defective ground plane structure at the ground plane parallel to feedline enhances the impedance matching at desired dual-band frequencies.

Table 1. Unit cell dimensions of the antenna.

Parameter	L_1	L_2	L_3	L_4	L_5	L_6	L_7	L_8	L_9
Length (mm)	31.5	11.7	7	2	4.8	1.3	11.05	5.2	8.52
Parameter	W_1	W_2	W_3	W_4	W_5	W_6	W_7	W_8	W_9
Length (mm)	26	3.2	7.85	7.03	6	1.4	6.8	1.2	3.38

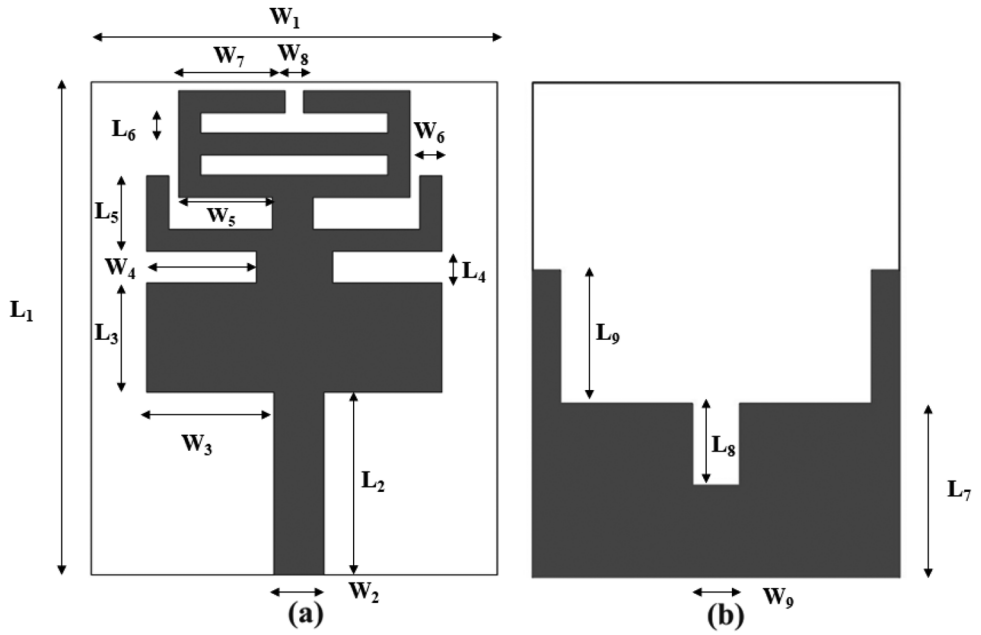

Figure 1. Top loaded Dual-band antenna (a) Radiator, (b) Ground Plane.

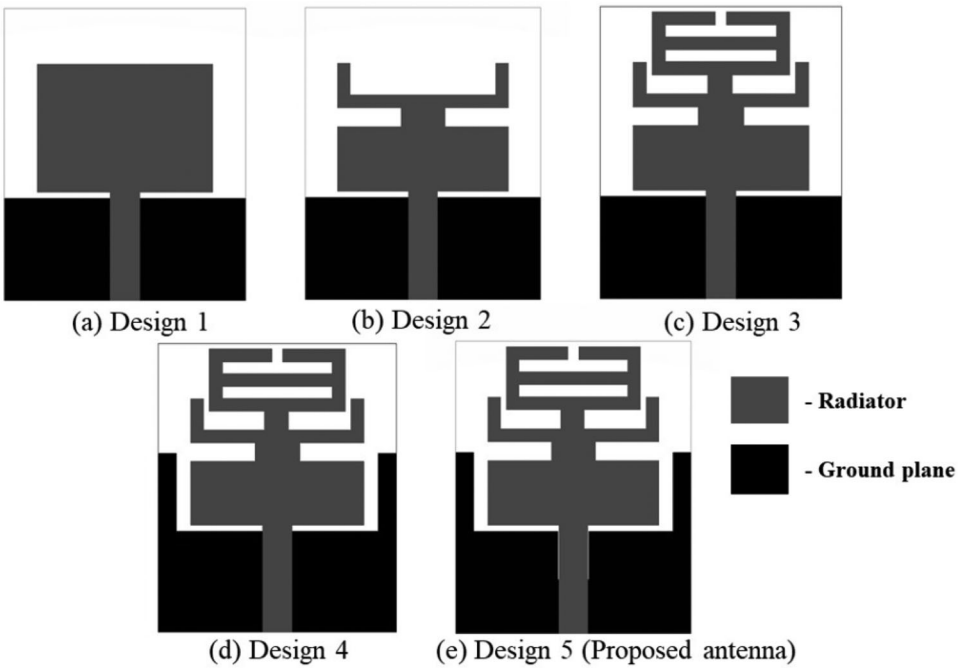

Figure 2. Evolution Design stages of the antenna.

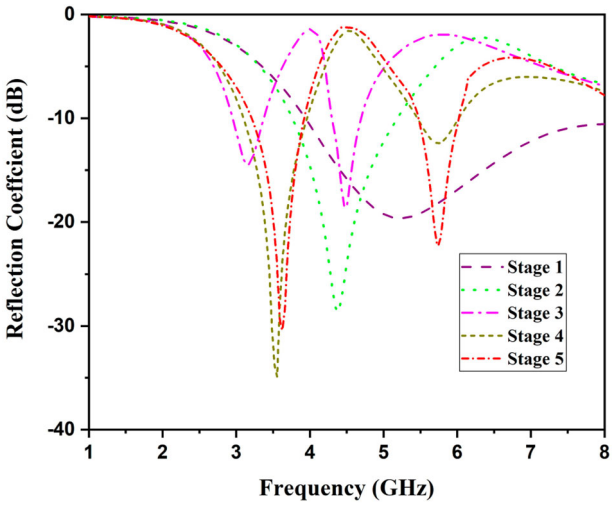

Figure 3. Reflection coefficient of the Antenna with evolution stages.

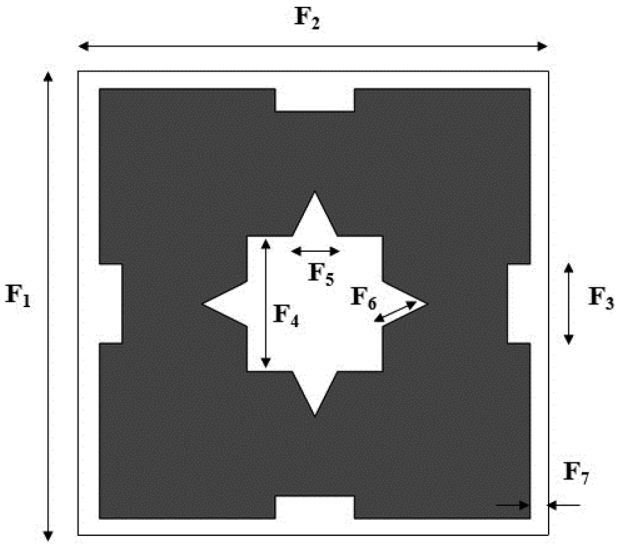

Figure 4. Frequency Selective Surface Unit cell design.

The simulated antenna has a bandwidth of 710 MHz between 3.21 GHz and 3.92 GHz in the n78 5G spectrum. It also spans the 5.54–6 GHz Wi-Fi spectrum, with 460 MHz bandwidth.

Table 2. Unit Cell dimensions of Frequency selective surface.

Parameter	F_1	F_2	F_3	F_4	F_5	F_6	F_7
Value (mm)	38.5	38.5	7	12	4	4.47	0.25

3. Frequency-selective surface design

A frequency-selective surface is a passive device that acts as a band-stop filter to reject unwanted frequencies. It also functions as a reflector, reducing back radiation and increasing antenna gain in the chosen direction. The square loop-inspired loop is fabricated on the same denim Jean substrate that was used to fabricate antenna [29]. Figure 4 depicts the Frequency Selective Surface unit cell design. Table 2 shows the unit cell size of FSS.

The resonance frequency formula for the square loop is mentioned in Equation 1. The perfect electric conductor, such as the copper portion present in FSS, produces inductance (L), whereas the separation of FSS unit cell distance and thickness results in capacitance (C).

$$f = \frac{1}{2\pi\sqrt{LC}} \tag{1}$$

The resonance frequency of frequency selective surface majorly depends on reactance and susceptance components present in the FSS structure [23]. The resonance

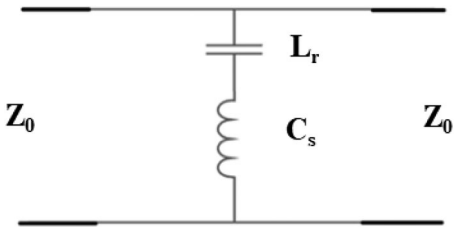

Figure 5. Equivalent circuit of FSS.

frequency equation of the presented FSS is mentioned in Equation 1

$$f_r = \frac{2\pi}{\sqrt{L_r C_s}} \tag{2}$$

The reactance portion of inductance (L_r) is caused by the wavelength of resonance frequency, the width of the conductor strip, and the periodicity of FSS. The Capacitance (C_s) portion of susceptance mainly depends on the gap ($2F_7$) between FSS array cells, periodicity, and wavelength.

The equivalent circuit of the FSS is depicted in Figure 5 [23]. The variation in gap between FSS cells, loop portion in FSS, and conductor portion in FSS contributes to the required resonance and bandwidth of transmission response. Figure 6 depicts the stages of FSS evolution. The transmission coefficient parameter of FSS is depicted in Figure 7. The square loop FSS is simulated on a denim Jean substrate with twice the wavelength of the resonance frequency, as shown in Figure 6(a), and yields resonance at 5.5 GHz.

As illustrated in Figure 6(b), a little rectangular patch part is deleted from four sides of the unit cell, which enhances the transmission coefficient value at the resonance frequency of 5.5 GHz. A square-shaped

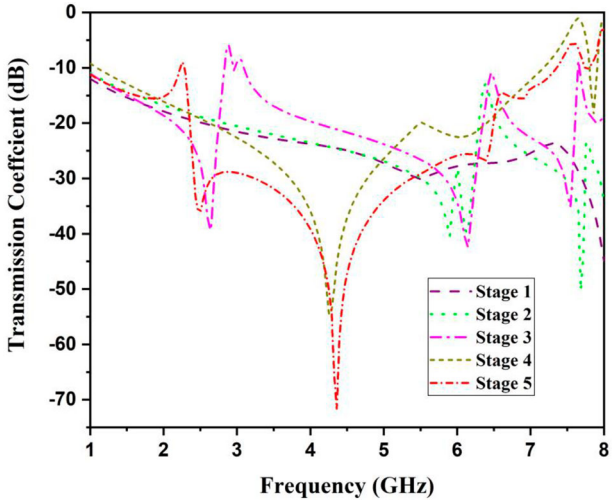

Figure 7. Transmission coefficient of Evolution stages of FSS.

portion is etched out from the centre of the unit cell and followed by the removal of the triangle portion at the four sides of the centre slot, as illustrated in Figure 6(c) and 6(d), respectively. The modification adopted in FSS increases the resonance length, which increases the inductance (L), as mentioned in eq. 1. In addition, the capacitance (C) is enhanced due to the square loop and triangular slot, which is employed in the FSS structure [25]. The increment in inductance and Capacitance leads to a reduction in resonance frequency. Stage 4 FSS produces a bandwidth of 2.54 GHz from 2.8 to 5.4 GHz. Furthermore, the patch of the top portion is replicated in the bottom portion of the FSS. This arrangement helps to enhance the bandwidth of FSS from 2.54–4.11 GHz with a frequency range of 2.35–6.46 GHz.

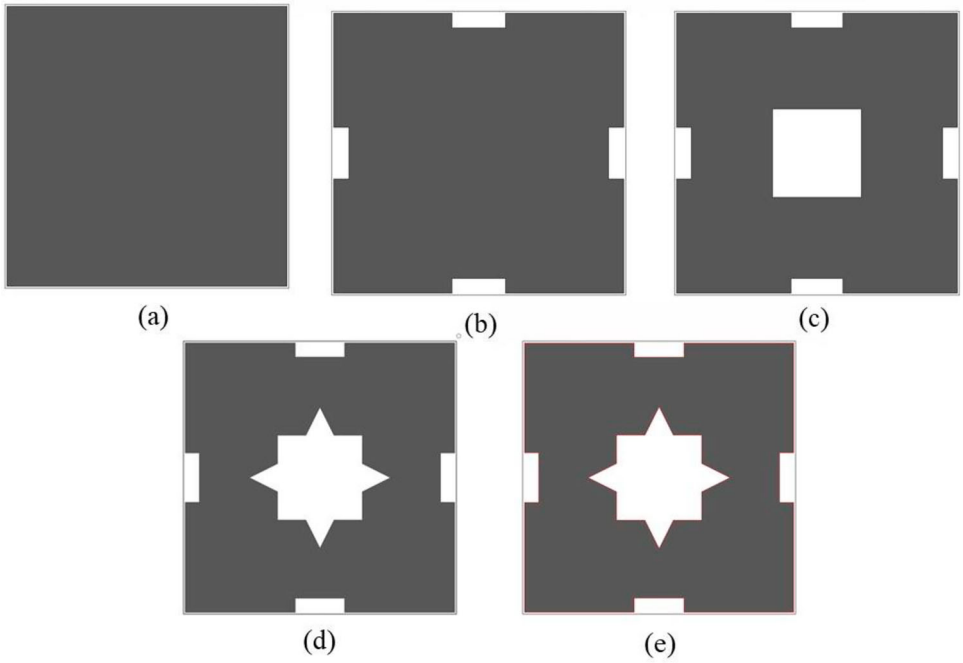

Figure 6. Evolution stages of Frequency Selective Surface (a) Stage 1, (b) Stage 2, (c) Stage 3, (d) Stage 4, (e) Stage 5.

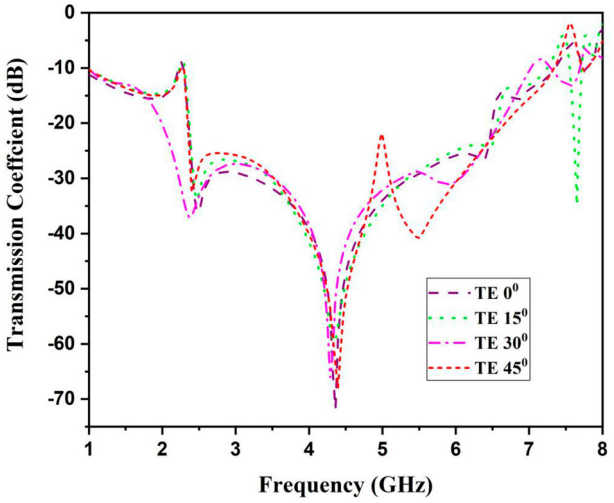

Figure 8. Transmission Coefficient of TE mode of polarization at different angles of incidence.

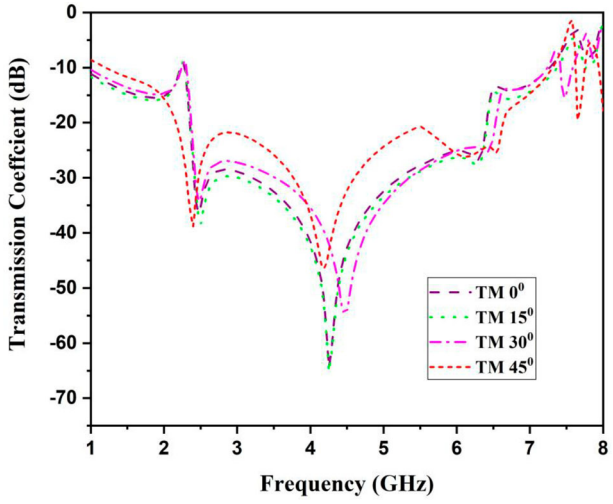

Figure 9. Transmission Coefficient of TM mode of polarization at different angles of incidence.

The stable transmission response at a different angle of incidence of the wave is required for the reflection nature of electromagnetic signals. The frequency response of frequency selective surface is expected to be insensitive to polarization modes at various angles of incidence. The frequency response of FSS at TE mode for various angles of incidence is shown in Figure 8.

At varying angles of incidence, the frequency response of a frequency-selective surface is predicted to be insensitive to polarization modes. Figure 9 depicts the frequency response of FSS in TE mode for various angles of incidence. Similarly, Figure 10 depicts the frequency response of FSS at TM mode with various angles of incidence [30]. It has been observed that a change in the angle of incidence up to 45° has a negligible impact on the transmission coefficient of square loop-inspired FSS. The stable transmission performance is observed up to 45° angle of incidence. Similarly, angular stability analysis for the FSS in TM mode was depicted in Figure 9. Due to the symmetric nature of FSS, it achieves stable transmission response up to 45°.

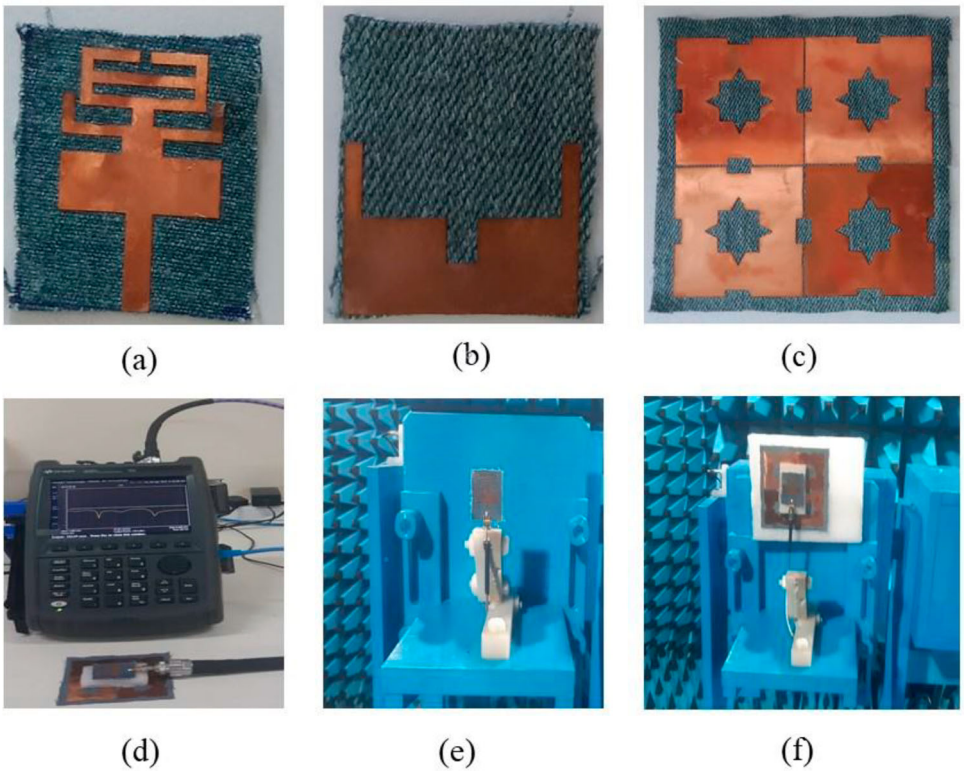

Figure 10. Prototype antenna and Measurement set-up (a) Radiator, (b) Ground Plane, (c) Frequency Selective surface, (d) reflection coefficient measurement of FSS-integrated antenna, (e) Anechoic chamber Antenna measurement set-up, (f) Anechoic chamber FSS-integrated Antenna measurement set-up.

4. Results and discussion

The top-loaded dual-band antenna radiator and the ground plane portion are etched out from a copper sheet with the aid of laser engraving technology. The radiator and ground plane portion of the antenna are embedded on denim Jean substrate by using conductive glue. The square loop-inspired FSS structure was created with laser engraving technology. The performance enhancement of the antenna is effective when the FSS array size is greater than that of the antenna size. The FSS with an array of 2 × 2 is chosen which has the size of 80 mm × 80 mm compared to the size of the antenna of 31.5 mm × 26 mm.

Figure 10 depicts the prototype antenna and measurement set-up. Figure 10 and 10(b) show the radiator and ground plane portion of the antenna, respectively. Figure 10(c) depicts the prototype structure of a 2 × 2 FSS array. Figure 10(d) depicts the reflection coefficient performance setup of an FSS-integrated antenna. The antenna anechoic chamber set-up and the FSS-integrated antenna are depicted in Figure 10(e) and 10(f), respectively.

FSS array size is increased from 2 × 2 to –4 × 4 and 8 × 8 and its gain performance is listed in Table 3. 2 × 2 array FSS which is placed behind the antenna gives the simulated peak gain of 8.37 dBi whereas 4 × 4 array FSS achieves the gain of 7.89dBi at 3.5 GHz [31]. A further increase in the array size of 8 × 8 gives a gain of 7.95dBi. The 2 × 2 FSS array (80 × 80 mm^2) itself larger than the actual antenna (31.5 × 26 mm^2) which is compelling enough to effectively reflect the back radiation. A further increase in FSS array size provides incremental gain which is achieved at the cost of an increased profile of the antenna [32]. In this work 2 × 2 array FSS gives 8.37 dBi gain which is higher than 4 × 4 and 8 × 8 array configurations.

4.1. Impedance characteristics

Figure 11 depicts the performance of the antenna's reflection coefficient. From Figure 11, it is observed that simulated values are validated with a measured response. The measured antenna has resonances at 3.5 and 5.8 GHz, with impedance bandwidths of 870 MHz and 350 MHz, respectively. The dual-band top-loaded antenna is bent along a 3.5 cm radius cylindrical foam and has a minor divergence in its reflection coefficient but covers the complete operational bandwidth. The

Table 3. Performance of the antenna with various FSS array configurations.

S.No	Number of arrays	FSS size	Gain (dBi) at 3.5GHz	Gain (dBi) at 5.8GHz
1	2 × 2	80 × 80 mm^2	8.37	6.55
2	4 × 4	160 × 160 mm^2	7.89	6.86
3	8 × 8	320 × 320 mm^2	7.95	6.97

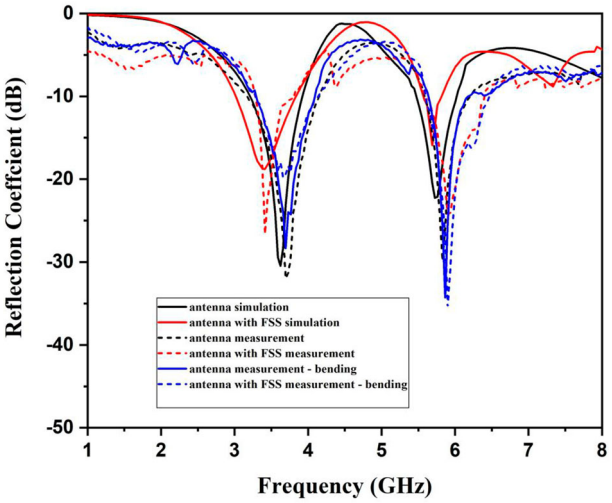

Figure 11. Reflection coefficient of the antenna.

bandwidth of the FSS integrated antenna is 620 MHz and 600 MHz at the resonance frequency of 3.5 and 5.8 GHz, respectively. The FSS-integrated antenna is likewise bent along the same cylindrical foam, which has no effect on the resonance frequency or impedance bandwidth.

4.2. Radiation characteristics

Figure 12 depicts the radiation parameters of an antenna and an FSS integrated antenna, as measured in an anechoic chamber model. Figure 12(a) and (b) show the E-plane pattern of an antenna and an FSS-integrated antenna at 3.5 and 5.8 GHz, respectively. It implies antenna has a bidirectional radiation pattern. Figures 12(c) and 11(d) show the H-Plane pattern of an antenna and the FSS-integrated antenna at 3.5 and 5.8 GHz, respectively.

It is observed that the antenna has the omnidirectional pattern at 3.5 and 5.8 GHz. The FSS array acts as a reflector, as shown in Figure 12(c) and Figure 12(d). The back radiation of the antenna is suppressed by the FSS array structure effectively. Table 4 shows the measured peak gain of the antenna and the FSS combined antenna. The antenna is enhanced by the amount of 5.18 dB at 3.5 GHz and 2.2 dB at 5.8 GHz.

The distance (d) between the antenna and FSS varied from 1 to 20 mm and its reflection coefficient is depicted in Figure 13. For the 1 mm separation distance, the antenna produces resonance at 2.4 GHz and 3.7 GHz whereas with the separation distance of 5 mm, the antenna exhibits a dual band of resonance at 2.5 GHz & 3.7 GHz. The antenna exhibits resonances of 2.8, 3.65 and 5.8 GHz when FSS is separated with a distance of 10 mm. Antenna with the FSS separation distance of 15 mm delivers resonance at 3.6 and 5.8 GHz with minimal peak reflection coefficient requirement. When the FSS is placed behind, the antenna with a separation distance of 20 mm produces the desired dual-band resonance at 3.5 and 5.8 GHz.

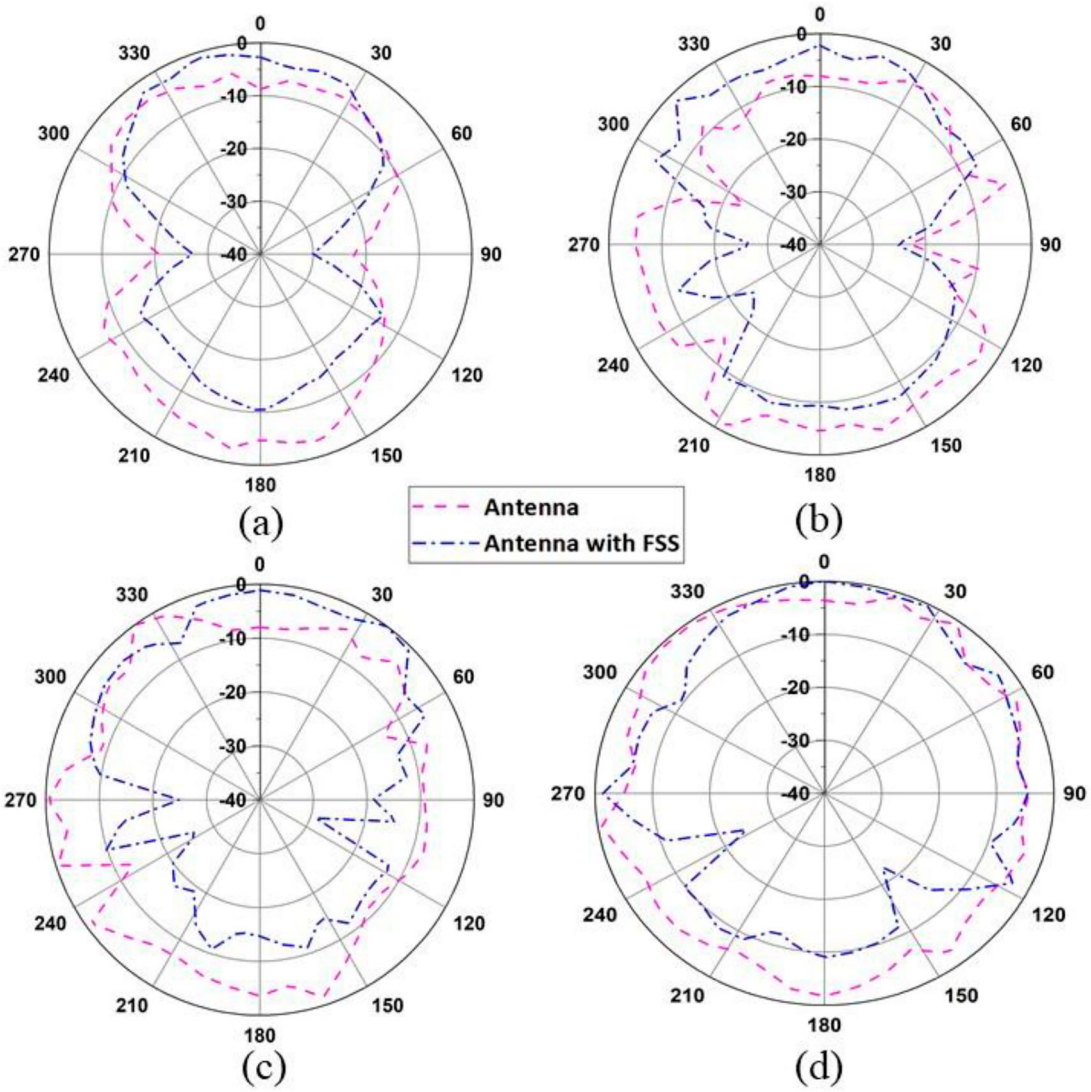

Figure 12. The radiation pattern of the antenna and FSS-integrated antenna (a) E-Plane at 3.5 GHz, (b) E-Plane at 5.8 GHz, (c) H-Plane at 3.5 GHz (d) H-Plane at 5.8 GHz.

Table 4. Measured gain of the antenna and FSS-integrated antenna.

Particular	Gain (dB) at 3.5 GHz	Gain (dB) at 5.8 GHz
Antenna	2.6	3.8
FSS integrated antenna	7.78	6.02

An FSS integrated antenna is placed on a cylindrical foam layer which has a radius of 2.5 cm, 3.0 cm and 3.5 cm. The antenna is bent along the x direction and the y-direction and its reflection coefficient is depicted in Figure 13. From the graph, it is observed that a slight variation in resonance frequency is observed with modification in the peak reflection coefficient. The FSS integrated antenna achieves the desired resonance at both the 3.5 GHz band and 5.8 GHz due to its perfect impedance-matching design.

The front-to-back ratio (FBR) of the FSS integrated antenna at 3.5 GHz is 14 dB whereas the FBR of 12.9 dB is observed at the resonance frequency of 5.8 GHz. The higher FBR validated better band rejection at the desired frequency with reduced back radiation due to the placement of FSS array structures (Figure 14).

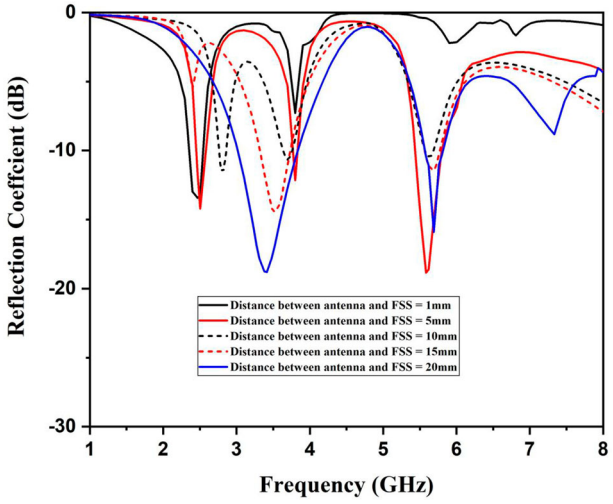

Figure 13. Reflection coefficient of the FSS-integrated antenna with d = 1, 5, 10, 15 and 20 mm.

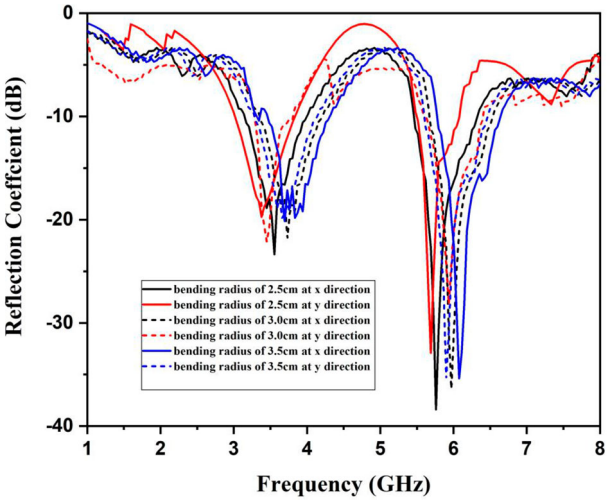

Figure 14. Reflection coefficient analysis of bending of the antenna at x and y directions.

4.3. SAR analysis

The antenna is aimed to validate body area communication where the specific absorption rate is a critical parameter to evaluate. The Specific Absorption Rate provides information on the amount of radiation absorbed by human body tissues [23]. The antenna and FSS combined antenna are placed on a human arm model, which has the electrical properties of skin, fat, muscle and bone modelled and placed beneath the antenna and FSS integrated antenna. The SAR values are depicted in Table 5.

The acceptable value of SAR by the FCC is 1.6W/Kg. The antenna without FSS produces higher FSS, which may create an impact on the human body tissues for continuous exposure to the radiation [24]. By positioning the FSS 10 mm below the antenna at 3.5 GHz, the SAR value is lowered from 2.51 to 0.370 W/Kg. At 5.8 GHz, the SAR value is reduced from 2.51 to 0.834W/Kg, which is an acceptable SAR value.

The distance between the 2 × 2 FSS configuration and antenna is varied between 1and 20 mm and its SAR and Gain performance is analysed, as listed in Table 6.

It is observed that the SAR value is above 1.6 W/Kg for the FSS separation distance up to 15 mm. When FSS is placed 20 mm below the antenna it provides acceptable SAR levels of 0.37 W/Kg and 0.834 W/Kg at 3.5 and 5.8 GHz, respectively. The gain of the FSS integrated antenna is increased as the separation distance between FSS and the antenna is increased. The simulated Peak gain of 8.37 dBi and 6.55 dBi is achieved at the resonance frequency of 3.5 and 5.8 GHz, respectively.

Table 5. Simulated SAR Values.

Particular	SAR (W/Kg) at 3.5 GHz	SAR (W/Kg) at 5.8 GHz
Antenna	2.51	2.51
FSS-integrated antenna	0.370	0.834

Table 6. SAR and Gain of FSS-Integrated antenna.

S.No	FSS and Antenna separation distance (mm)	SAR at 3.5 GHz (W/Kg)	SAR at 5.8 GHz (W/Kg)	Gain at 3.5 GHz (dBi)	Gain at 5.8 GHz (dBi)
1	1	4.2	5.2	4.79	3.19
2	5	3.4	3.2	5.29	4.93
3	10	2.2	2.6	6.36	5.74
4	15	1.7	1.62	7.02	6.12
5	20	0.37	0.834	8.37	6.55

5. Conclusion

An innovative compact dual-band wearable antenna for 5G and Wi-Fi applications is presented in this article. The antenna is 31.5 mm × 26 mm and is made of a flexible denim Jean substrate. Frequency selective surface improved the performance of the antenna that has 38.5 mm × 38.5 mm unit cell dimensions. The FSS-integrated antenna has a bandwidth of 620 MHz and 600 MHz at resonance frequencies of 3.5 and 5.8 GHz, respectively. The FSS-integrated antenna further improved the gain of the antenna by 7.78 dB and 6.02 dB at 3.5 and 5.8 GHz, respectively. The FSS-integrated antenna also provides an acceptable SAR level and optimal performance in the bending condition. Because of the FSS array's reflective nature, the antenna performs better and has a significant reduction in SAR level. This antenna system stands out among all existing antenna systems due to its compact profile, stable impedance characteristics, improved gain performance and reduced SAR. The proposed antenna is a good candidate for wireless body area communication applications that require a short range. A wearable FSS antenna that is multiband, including ISM, UWB and 5G standards, will be designed in future.

Disclosure statement

No potential conflict of interest was reported by the author(s).

References

[1] Çelenk E, Tokan NT. All-textile on-body antenna for military applications. IEEE Antennas Wirel Propag Lett. May 2022;21(5):1065–1069. doi:10.1109/LAWP.2022.3159301

[2] Ali U, Ullah S, Kamal B, et al. Design, analysis and applications of wearable antennas: a review. IEEE Access. 2023;11:14458–14486. doi:10.1109/ACCESS.2023.3243292

[3] Ashyap AYI, et al. An overview of electromagnetic band-gap integrated wearable antennas. IEEE Access. 2020;8:7641–7658. doi:10.1109/ACCESS.2020.2963997

[4] Althuwayb AA, et al. Metasurface-inspired flexible wearable MIMO antenna array for wireless body area network applications and biomedical telemetry devices. IEEE Access. 2023;11:1039–1056. doi:10.1109/ACCESS.2022.3233388

[5] Wang Z, Wang M, Nie W. Design of a dual-band WiFi antenna using the theory of characteristic modes

and nested Chinese characters. Electronics (Basel). 2023;12:3465. doi:10.3390/electronics12163465

[6] Nelaturi S, Raja AS, Rakesh Y. Dual- band antenna for Wi-Fi and 5G applications. Int J Eng Adv Technol. 2019;9(1s5):130–131. doi:10.35940/ijeat.A1032.1291S519

[7] An W, Tian X, Wang J, et al. Low-profile dual-polarized double-layer microstrip antenna for 5G and 5G Wi-Fi. Micromachines (Basel). 2023;14:942. doi:10.3390/mi14050942

[8] Yu Z, et al. A wearable self-grounding slit antenna for ISM/4G/5G/bluetooth/WLAN applications. IEEE Access. 2023;11:87930–87937. doi:10.1109/ACCESS.2023.3305258

[9] Musa U, et al. Design and analysis of a compact dual-band wearable antenna for WBAN applications. IEEE Access. 2023;11:30996–31009. doi:10.1109/ACCESS.2023.3262298

[10] Le and T TT, Yun -Y. Wearable dual-band high-gain low-SAR antenna for off-body communication. IEEE Antennas Wirel Propag Lett. July 2021;20(7):1175–1179. doi:10.1109/LAWP.2021.3074641

[11] Yang H, Liu X. Wearable dual-band and dual-polarized textile antenna for on- and off-body communications. IEEE Antennas Wirel Propag Lett. Dec. 2020;19(12):2324–2328. doi:10.1109/LAWP.2020.3032540

[12] Kapoor A, Mishra R, Kumar P. Complementary frequency selective surface pair-based intelligent spatial filters for 5G wireless systems. J Intell Syst. 2021;30(1):1054–1069. doi:10.1515/jisys-2021-0082

[13] Zhu H, Yu Y, Li X, et al. A wideband and high gain dual-polarzied antenna design by a frequency-selective surface for WLA application. Prog Electromag Res C. 2014;54:57–66. doi:10.2528/PIERC14072801

[14] Hussin F, Ahmad B, Aziz A, et al. (2016). Design and impedance modeling for dual band and multiple band frequency selective surface (FSS). 94–99. doi:10.1109/APACE.2016.7916483.

[15] Kapoor A, Mishra R, Kumar P. Novel wideband frequency selective surface based space borne filters for sub-6 GHz 5G devices. 2021 4th Biennial International Conference on Nascent Technologies in Engineering (ICNTE), Navi Mumbai, India, 2021, pp. 1–6. doi:10.1109/ICNTE51185.2021.9487649

[16] Krachodnok P. A dual band microstrip patch antenna for WLAN and WiMAX applications. World Acad Sci Eng Technol Int J Electron Commun Eng. 2014;8(7):1057–1061.

[17] Fernandes E, Silva M, Briggs L, et al. 2.4-5.8 GHz Dual-Band patch antenna with FSS reflector for radiation parameters enhancement. AEU – Int J Electron Commun. 2019;108. doi:10.1016/j.aeue.2019.06.021

[18] Shi C, Zou J, Gao J, et al. Gain enhancement of a dual-band antenna with the FSS. Electronics (Basel). 2022;11:2882. doi:10.3390/electronics11182882

[19] Li Q, Liu Z-G, Lu W-B, et al. Dual-band and dual-polarization base station antennas integrated with FSS, baffle, and notched director. 2021 International Conference on Microwave and Millimeter Wave Technology (ICMMT), Nanjing, China, 2021, pp. 1–3. doi:10.1109/ICMMT52847.2021.9618250

[20] Ashyap AYI, et al. Highly efficient wearable CPW antenna enabled by EBG-FSS structure for medical body area network applications. IEEE Access. 2018;6:77529–77541. doi:10.1109/ACCESS.2018.2883379

[21] Alwareth H, Ibrahim IM, Zakaria Z, et al. A wideband high-gain microstrip array antenna integrated with frequency-selective surface for Sub-6 GHz 5G applications. Micromachines (Basel). 2022;13:1215. doi:10.3390/mi13081215

[22] Tewary T, Maity S, Roy A, et al. Wide band microstrip patch antenna with enhanced gain using FSS structure. J Microw Optoelectron Electromag Appl. 2023;22(2):329–345. doi:10.1590/217910742023v22i2273333

[23] Sugumaran B, Balasubramanian R, Palaniswamy SK. Performance evaluation of compact FSS-integrated flexible monopole antenna for body area communication applications. Int J Commun Syst. 2022: e5085. doi:10.1002/dac.5085

[24] Das P, Mandal K. Modelling of ultra-wide stop-band frequency-selective surface to enhance the gain of a UWB antenna. IET Microw Antennas Propag. 2019;13(3):269–277. doi:10.1049/iet-map.2018.5426

[25] Das P, Mandal K. RCS reduction of microstrip antenna using split square loop thin absorber. IET Microw Antennas Propag. 2020;14(14):1771–1778. doi:10.1049/iet-map.2020.0347

[26] Hu Z, Xiao Z, Jiang S, et al. A dual-band conformal antenna based on highly conductive graphene-assembled films for 5G WLAN applications. Materials (Basel). 2021;14(17):5087. doi:10.3390/ma14175087

[27] Yang SJ, Zhang XY. Frequency selective surface-based dual-band dual-polarized high-gain antenna. IEEE Trans Antennas Propag. 2021;70(3):1663–1671. doi:10.1109/TAP.2021.3111222

[28] Saleem R, Bilal M, Chattha HT, et al. An FSS based multiband MIMO system incorporating 3D antennas for WLAN/WiMAX/5G cellular and 5G Wi-Fi applications. IEEE Access. 2019;7:144732–144740. doi:10.1109/ACCESS.2019.2945810

[29] Xiao Y, Zu H, Song R, et al. Multi-band and low specific absorption rate wearable antenna with low profile based on highly conductive graphene assembled film. IEEE Antennas Wirel Propag Lett. 2023.

[30] Das P, Mandal K. Hybrid frequency selective surface phase cancelation structure based broadband switchable radar cross section reduction. Int J RF Microw Comput-Aid Eng. 2021;31(3):e22554.

[31] Ayaz M, Ullah I. A phased array antenna with novel composite right/left-handed (CRLH) phase shifters for Wi-Fi 6 communication systems. Appl Sci. 2023;13(4):2085. doi:10.3390/app13042085

[32] Devarapalli AB, Moyra T. CPW-fed dual-element metamaterial inspired multiband antenna using simple FSS for gain enhancement. Optik (Stuttg). 2023;290:171313. doi:10.1016/j.ijleo.2023.171313